# Density of states within the bandgap of perovskite thin films studied using the moving grating technique

F. Ventosinos[1,2], A. Moeini[3], D. Pérez-del-Rey[3], H. Bolink[3], J.A. Schmidt[1,2]

[1]Instituto de Física del Litoral (IFIS-Litoral), CONICET-UNL, Güemes 3450, S3000GLN Santa Fe, Argentina

[2]Facultad de Ingeniería Química, Universidad Nacional del Litoral, Santiago del Estero 2829, S3000AOM Santa Fe, Argentina

[3]Instituto de Ciencia Molecular, Universidad de Valencia, C/Catedrático J. Beltrán 2, 46980 Paterna, España

**Abstract**

In this work, we further study the moving grating technique applied to halide perovskite thin film materials. Firstly, we show some problems that emerge when analyzing experimental data with the classical formulation, which does not distinguish between free and trapped carriers and hence only gives average quantities for the transport parameters. We show that using a more general framework, taking into account the multiple trapping of carriers within a density of localized states, allows for accurate description. Since it includes the density of state (DOS) of the material, it enables the possibility of testing different DOS models proposed in the past for halide perovskite thin films. We check if these models give rise to the type of curves that we have measured under different experimental conditions. Finally, we propose a new model for the DOS in the forbidden gap, which results in the best fit found for the measurements performed. This allows us to give ranges of values for the parameters defining the DOS, that, to our knowledge, are given for the first time.

## I. INTRODUCTION

The incredible success of emerging perovskite materials in the last 10 years has made them a candidate for low-cost high-efficiency solar cells. Despite the increasing performance of perovskite solar cells and the improved stability, the precise transport phenomena taking place in the absorber material are still under investigation. To study this type of phenomena, several techniques have been used, which can be separated into two large groups: transient techniques and steady-state techniques. Recently [1], it was suggested that steady-state techniques are better suited for materials used as absorbers in solar cells, since the parameters extracted from pulsed techniques may be misinterpreted. In a previous publication [2] we have shown that the steady-state moving grating technique (MGT) can be applied to halide perovskites (HaPs), giving very useful information on the drift mobilities of both type of carriers and the recombination lifetime. The general idea of the MGT technique is to illuminate the sample with two coherent light beams, generating an interference pattern over a sample with coplanar geometry. Introducing a slight frequency difference between both beams, the pattern is not static but moves at a constant speed, $v_{gr}$. The movement of this light pattern generates a short circuit photocurrent, $j_{sc}$, even in the absence of an external electric field. Varying the speed of the grating and recording the short circuit current, generates a curve from which the transport parameters can be obtained [2].

In this work we continue studying the MGT; in particular we focus on the mathematical treatment to deduce the dependence of $j_{sc}$ as a function of $v_{gr}$. In the original publication[3,4] the authors proposed a treatment that does not distinguish between trapped and free carriers. This simplification allowed them to arrive to a compact expression with three fitting parameters, both mobilities ($\mu_P$, the hole drift mobility, and $\mu_N$, the electron drift mobility) and the common recombination lifetime, $\tau_R$. We have found that this simplified treatment may be the reason not only for the indetermination of the minority carrier mobility (usually, the error of the fitted mobility is larger than the value), but also for the incorrect results obtained in some measurements performed at different grating periods (see figure 1). To solve these issues, we propose to use a more general framework that distinguishes between free carriers, $n(x,t)$ and $p(x,t)$, and trapped carriers, $n_t(x,t)$ and $p_t(x,t)$, by calculating their concentrations via the introduction of the density of states (DOS) of the semiconductor. After showing that our formalism solves the issues found, we explore how the measurements of the moving grating technique can be used to test some DOS models for perovskite materials found in the literature, and may help to gain insight on the transport phenomena in HaPs.

## II. METHODS

### A. Original treatment of the moving grating technique

The MGT was introduced in the early 90s by Haken, Hundhausen and Ley [3,4] for the study and characterization of hydrogenated amorphous silicon. Starting from the total concentrations of carriers, free plus trapped, the authors derived an expression of the photocurrent density as function of $v_{gr}$ that can be written:

$$j_{sc}(v_{\mathrm{gr}}) = \frac{c_1 v_{\mathrm{gr}}}{c_2 + c_3 v_{gr}^2 + c_4 v_{gr}^4} \quad , \tag{1}$$

with the following definitions:

$$c_1 = \frac{q^2}{2\varepsilon\varepsilon_0} (g_{ac}\, \tau_R\, k)^2 \, \frac{kT}{q} \, (\mu_N + \mu_P)\, (\mu_N - \mu_P) \, ,$$

$$c_2 = {\tau_R}^{-2} \left[ \left( a + \frac{(b+1)^2}{4b} \, l^2 \right) (1 + l^2) \right]^2 ,$$

$$c_3 = k^2 \left[ 1 + a^2 + \frac{\left( (b+1)^2 + 2a(b^2+1) \right)}{2b} l^2 + \frac{(b+1)^2 (b^2+1)}{4b^2} \, l^4 \right],$$

$$c_4 = k^4 {\tau_R}^2 \, .$$

In these equations, $q$ is the absolute value of the electron charge, $kT$ is the thermal energy, $g_{ac} = 2\sqrt{G_1 G_2}$ ($G_1$ and $G_2$ are the generation rates corresponding to beams 1 and 2 alone, respectively), $k$=2π/$\Lambda$ is the spatial frequency, and the short-hand notations $a$, $b$ and $l$ are:

$$a = \frac{\tau_R}{\tau_{diel}}\ ; \quad b = \frac{\mu_N}{\mu_P}; \quad l = k\sqrt{\tau_R D_{amb}}; \quad D_{amb} = 2\,\frac{kT}{q}\,\frac{\mu_N \times \mu_P}{(\mu_N + \mu_P)},$$

with $\tau_{diel}$ being the dielectric relaxation time. Therefore, there are only three free parameters, both mobilities $\mu_N$ and $\mu_P$ and the common recombination lifetime $\tau_R$. Since the carrier concentrations are average quantities in this formalism, the fitted mobilities correspond to the drift mobilities, and the recombination lifetime is the total time spent by the carriers since their creation until recombination, including the time spent in trap states. As it was discussed in our recent publication [2], fitting MGT curves, both for hydrogenated amorphous silicon and for HaPs films, with Eq. (1) has some weaknesses. On the one hand, trying to use the 3 parameters to achieve the fit may result in an indetermination for the values of the parameters, as the errors are larger than the parameters themselves. This happened in our previous study for several grating periods and generation rates, in both types of materials. To fix this issue, we proposed using the measured photoconductivity to express the minority carrier mobility in term of the majority carrier mobility and the recombination lifetime, hence fitting with only 2 parameters. This improved the fitting, giving results with an error below 5% for both fitted parameters.

On the other hand, we have found that Eq. (1) gives incorrect results when trying to fit curves measured with different grating periods, as shown in Figure 1. The data presented are measurements done at room temperature on a HaPs (MAPI) film with a generation rate $G_0 = 4.3\times10^{21}$ cm$^{-3}$s$^{-1}$; further details of the sample will be given in the experimental section.

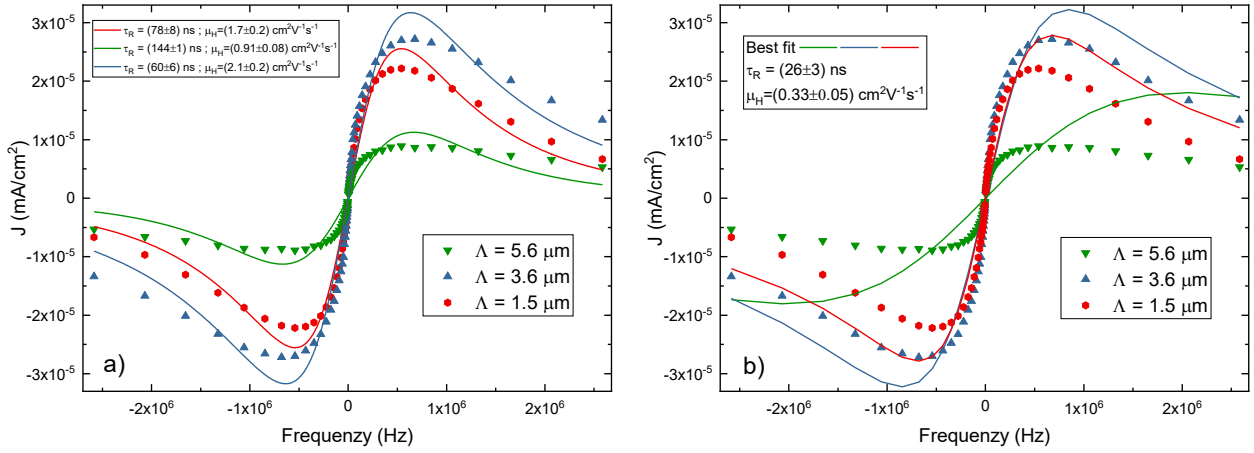


*Figure 1: Result of applying the fitting procedure suggested in Ref. [1] to a HaP. a) Each curve is fitted individually, giving good overall fit but different transport parameters for each case; b) The fitting procedure is carried on trying to find the best transport parameters for all the three curves, giving worse overall fit.*

As can be seen from figure 1 a), a decent fit of all the three curves can be obtained if we fit each one individually, but this results in three different sets of transport parameters. Since all three measurements were made at the same temperature and generation rate, it is expected that the drift mobilities and the recombination lifetime to be the same. If we force the fitting routine to fit all three curves with only one set of parameters, the quality of the fitting diminishes quite strongly, as seen in figure 1 b). This result shows that the theoretical framework used in the original publication has some limitations. In order to improve the analysis of the experimental data that is generated in the MGT, in the next section we propose a more general treatment of the equations, distinguishing between trapped and free carriers by means of the DOS.

**B. Theoretical treatment based on the density of states**

In order to account for free and trapped carriers, we shall introduce the DOS in the forbidden gap for the material, *N(E)*. As we have done in previous reports [5,6], we will start with a simple model consisting on monovalent states having all the same capture coefficients. The generalization to different species of states having different capture coefficients is straightforward. The generation rate for an interference pattern that travels at a constant speed may be written as:

$$G_{MGT} = G_0 + \Delta G_0 \cos(k\,x + \Delta\omega\,t) = G_0 + Re\{\Delta G_0 e^{j(k\,x\,+\,\Delta\omega\,t)}\}, \tag{2}$$

where $\Delta\omega$ is the angular frequency difference between the interfering beams, $\Delta\omega = 2\pi\Delta f$ (which is related to the grating speed by $v_{gr}=\Lambda\cdot\Delta f$), $x$ is the spatial coordinate in the plane of the sample perpendicular to the contacts, $t$ is the temporal variable, $Re$ designates the real part of a complex number, and $j$ is the imaginary unit. Consequently, the generation rates in equation (2) are given by $G_0 = G_1 + G_2$ and $\Delta G_0 = 2\gamma_0\sqrt{G_1\,G_2}$, $\gamma_0$ is the interference quality factor; its value is positive and less than one as a consequence of light scattering, mechanical vibrations, and the partial coherence of the beams.

When there is a large difference between the beams' photon generation rates, the condition $\Delta G_0 \ll G_0$ is fulfilled, which allows discarding the higher-order terms in the equations. In steady state, consequently, the harmonic generation rate produces free photocarrier densities with the same functional dependence on the variables, according to the continuity equations:

$$\frac{\partial n(x,t)}{\partial t} = G(x,t) - R_n(x,t) + \frac{1}{q}\frac{\partial}{\partial x}\left[j_n(x,t)\right], \tag{3}$$

$$\frac{\partial p(x,t)}{\partial t} = G(x,t) - R_p(x,t) - \frac{1}{q}\frac{\partial}{\partial x}\left[j_p(x,t)\right], \tag{4}$$

In these equations, $n(x,t)$ and $p(x,t)$ are the free concentrations of electrons (in the conduction band) and holes (in the valence band), respectively, $R(x,t)$ denotes the recombination rate, while $j(x,t)$ is the total current. As in the rest of this work, the subscript *n* refers to electrons and the subscript *p* to holes. Since the experiment is performed without an external electric field, the current is generated via an internal electric field $\xi_{int}(x,t)$ that develops according to Poisson´s equation:

$$\frac{d\xi_{int}(x,t)}{dx} = \frac{q}{\varepsilon\varepsilon_0}\begin{Bmatrix} p(x,t) + \int_{E_v}^{E_c}[1 - f(E,x,t)]N^{DON}(E)dE + N_d \\ -n(x,t) - \int_{E_v}^{E_c} f(E,x,t)N^{ACC}(E)dE - N_a \end{Bmatrix}, \tag{5}$$

where $\varepsilon$ is the dielectric constant of the sample, $\varepsilon_0$ is the dielectric permittivity of vacuum, $E_v$ is the energy at the top of the valence band, $E_c$ is the energy at the bottom of the conduction band, $f(E,x,t)$ is the occupation function, $N^{DON}(E)$ is the density of donor defect states (neutral when occupied and positively charged when unoccupied), $N_d$ is the density of external donor dopants (assumed completely ionized and therefore positively charged), $N^{ACC}(E)$ is the density of acceptor defect states (neutral when empty and negatively charged when occupied), and $N_a$ is the density of external acceptor dopants (assumed completely ionized and therefore negatively charged). As can be seen, this internal electric field

is comprised of free plus trapped charge. In amorphous materials such as hydrogenated amorphous silicon, the trapped charge is much higher than the free carriers, hence dominating the internal electric field. For HaPs we cannot make such an assumption, since the exact DOS distribution within the bandgap of this material is still under discussion. Taking this into account we will continue developing the general equations, while in the next sections we will use different DOS models already proposed in the literature, solving the equations using a computer code to compute the $j_{sc}(v_{gr})$ curves and comparing with measurements.

The recombination terms can be written as

$$R_n(x,t) = \int_E^E \left\{ c_n n(x,t) \left[ 1 - f(E,x,t) \right] - e_n(E) f(E,x,t) \right\} N(E)\, dE\,, \tag{6}$$

$$R_p(x,t) = \int_E^E \left\{ c_p p(x,t) f(E,x,t) - e_p(E) \left[ 1 - f(E,x,t) \right] \right\} N(E)\, dE\,, \tag{7}$$

where *c* is the capture coefficient, *e(E)* is the emission rate and *N(E)* is the DOS. The current densities are the sum of the drift and diffusion components

$$j_n(x,t) = q\ \mu_n\ n(x,t)\, \xi(x,t) + q\ D_n\ \frac{\partial n(x,t)}{\partial x}\quad , \tag{8}$$

$$j_p(x,t) = q\ \mu_p\ p(x,t)\, \xi(x,t) - q\ D_p\ \frac{\partial p(x,t)}{\partial x}\quad , \tag{9}$$

where $\mu$ is the extended-states mobility, *D* is the diffusion coefficient and $\xi(x,t)$ is the electric field, which for this case is only comprised of the internally developed electric field (the experiment is performed in short-circuit conditions, but a general case would add an external power source also). In order to solve equations (3)-(5), we recall that in the low modulation condition ($G_1 >> G_2$) it is expected that the relevant physical parameters vary sinusoidally as $G(x,t)$ does. In general, however, there will be variable phase shifts, and any quantity *A* can be expressed as $A(x,t) = A_0 + \Re e\left[\ \delta A\quad e^{i(kx+\omega t)}\ \right]$, where $A_0$ is the value under uniform illumination $G_0$, and $\delta A$ is a complex magnitude originating from the modulated term of the generation rate $\delta G$. Introducing these expressions for $n(x,t)$, $p(x,t)$ and $\xi(x,t)$ into the differential equations (3)-(9) linearizes them, giving rise to a system of linear complex equations. Once the quantities $n(x,t)$ and $p(x,t)$ are known, the current density can be calculated via

$$\Delta J_{MGT} = \frac{1}{2} Re\left\{ \Delta\sigma_{\Delta\omega,k}\ \Delta\xi^*_{\Delta\omega,k} \right\}, \tag{10}$$

where the photoconductivity amplitude, $\Delta\sigma_{\Delta\omega,k}$, is proportional to the amplitudes of the free photocarrier densities:

$$\Delta\sigma_{\Delta\omega,k} = q\left(\mu_n\, \Delta n_{\Delta\omega,k} + \mu_p\, \Delta p_{\Delta\omega,k}\right). \tag{11}$$

The asterisk as superscript defines the complex conjugate of the number. A more general treatment that solves the transport equations for a slightly more general generation rate $G = G_0 + Re\{g_{\Omega,\mathrm{k}}\, e^{j(k\,x+\Omega\,\mathrm{t})}\}$ with $|g_\Omega| \ll G_0$, assuming valid the multiple-trapping model for the free carriers, can be found in [6].

In section 4, we will show the results of solving these equations for different *N(E)* distributions by means of numerical simulations.

**III. EXPERIMENTAL DETAILS**

The glass substrates, purchased from Naranjo Substrates, were cleaned with soap, deionized water, and isopropanol under an ultrasonic bath, followed by a UV-$O_3$ treatment. Then, the substrates were transferred to a vacuum chamber inside a $N_2$-filled glovebox for the perovskite deposition. The perovskite composition is $CH_3NH_3PbI_3$ (MAPI), and it was deposited by vacuum-deposition following a method previously described [7]. Summarizing, methylammonium iodide ($CH_3NH_3I$, Lumtec) and lead (II) iodide ($PbI_2$, Sigma Aldrich) powders are deposited separately in ceramic crucibles. The crucibles are heated up in high vacuum using Creaphys sources until the materials start subliming. By using quartz microbalance sensors one can accurately control the evaporation rate of each component. By using stoichiometric amounts of each component and controlling the perovskite thickness with a third sensor near the substrate we prepared 500-600 nm perovskite films. Then, the samples were transferred to another vacuum chamber to deposit gold pads for contacting. In this chamber the working principle for evaporation is similar but the heat is achieved by applying a high current input through a tungsten boat with gold beads. Finally, the samples were encapsulated with $Al_2O_3$ deposited by atomic layer deposition (ALD). Using this type of material, efficiencies around 18% have been obtained, as can be seen in figure 2 of [7].

We used a 10 mW He-Ne laser as a source of coherent light, while the short circuit current was measured with a Keithley 6514 system electrometer. Our setup allows measuring from 0.75 µm up to 6 µm of grating period, but with some improvement in the setup values in the order of 20 µm are easily achievable. For the experimental data presented, we measured each data point 20 times to calculate the average value and the standard error, while the waiting time after changing the grating velocity was set to 3 seconds.

**IV. RESULTS AND DISCUSSION**

In order to solve the balance equations and compute the photogenerated current density $j_{sc}$ as a function of the grating velocity $v_{gr}$, it is needed to define a density of states in the forbidden gap. Several authors have proposed different models for the DOS of HaPs, that have been used in simulation codes like AMPS-1D [8] and SCAPS [9] for instance, or to try to explain different experimental data. In this section, we will try some of these models to see if they give rise to a signal similar to the one observed in our experiments.

A. **Effective single type of capturing center**:

This model was proposed by Levine *et al*. [10], in order to explain the results obtained using photoconductivity and SSPG measurements. As expressed by these authors, the simplest model consistent with the measured dependence of the photoconductivity ($\sigma_{ph} \propto \mathrm{G_0}^{\gamma}$) and the ambipolar

diffusion length ($L_{amb} \propto {G_0}^{-S}$) on the generation rate, is a single trap level located a few *kT* above the Fermi level. From dark conductivity measurements they found a Fermi level close to 0.4 eV above the valence band, therefore they assume a trap level 0.6 eV above the valance band. In this work, we measured a room temperature dark conductivity $\sigma_{dark} = 1.3\ 10^{-8}\ \Omega^{-1} cm^{-1}$. To calculate the Fermi level from this dark conductivity we use $\sigma_{dark} = q\ p\ \mu_p$, where *p* is the number of holes in the valence band and $\mu_p$ the mobility of holes in the valence band. This expression is valid for a p-type semiconductor, which in our case is confirmed by the MGT experiment, sensitive to the doping as explained in [2]. The link between dark conductivity and the Fermi level comes from the equation $p = N_V e^{\left(\frac{E_V - E_F}{kT}\right)}$, which combined with the previous one gives $E_F - E_V = kT\ ln\left(\frac{q\ \mu_p\ N_V}{\sigma_{dark}}\right)$. Assuming the same values as in [10] for the hole mobility ($\mu_p = 1\ \frac{cm^2}{V\ s}$) and for the effective density of states at the valence band ($N_V = 2.4 \times 10^{18}\ cm^{-3}$), we arrive to a Fermi level situated 0.44 eV above de valence band, in accordance with the value quoted by Levine *et al*. [10].

In order to perform the simulation, the values of temperature, generation rate and grating period are fixed equal to those used during the measurements. The density of trap states, as well as the capture coefficients for electrons and holes, are taken as fit parameters. The trap DOS is modeled with a narrow Gaussian distribution of acceptor states, described by two parameters, the total concentration of traps, $N_t$, and the energetic position within the bandgap, $E_t$. This last parameter is restricted to be between 0.45 and 0.65 eV (i.e., a few kT above the Fermi level). The best fit is obtained for a density of acceptor traps $N_t$ = 7.2x10$^{15}$ cm$^{-3}$, located at $E_t$ = 0.62 eV above the valence band edge, while the capture coefficients are $c_n$=7.5x10$^{-10}$ cm$^3$s$^{-1}$ and $c_p$=7.5x10$^{-9}$ cm$^3$s$^{-1}$. The full set of parameters is given as supplementary information. The fact that $c_p > c_n$ is consistent with the acceptor nature of the trap. Indeed, the trap is neutral when it captures an electron, but it is negatively charged when it captures a hole, so in this last case the coulombic attraction increases the capture coefficient. As can be seen in figure 2, the fitted curves seem to be peaked at higher frequencies than the measured ones. We have chosen to show only the positive branch of the graph, displaying it in logarithmic scales in the horizontal axis, for the sake of clarity. Another thing to consider is if the chosen DOS is able to reproduce the measured values of dark and photo conductivities ($\sigma_{dark}$ and $\sigma_{ph}$). In our case, for the sample shown in figure 2, the experimental values of the conductivities are $\sigma_{dark}$=1.3x10$^{-8}$ (Ωcm)$^{-1}$ and $\sigma_{ph}$=2x10$^{-5}$ (Ωcm)$^{-1}$.

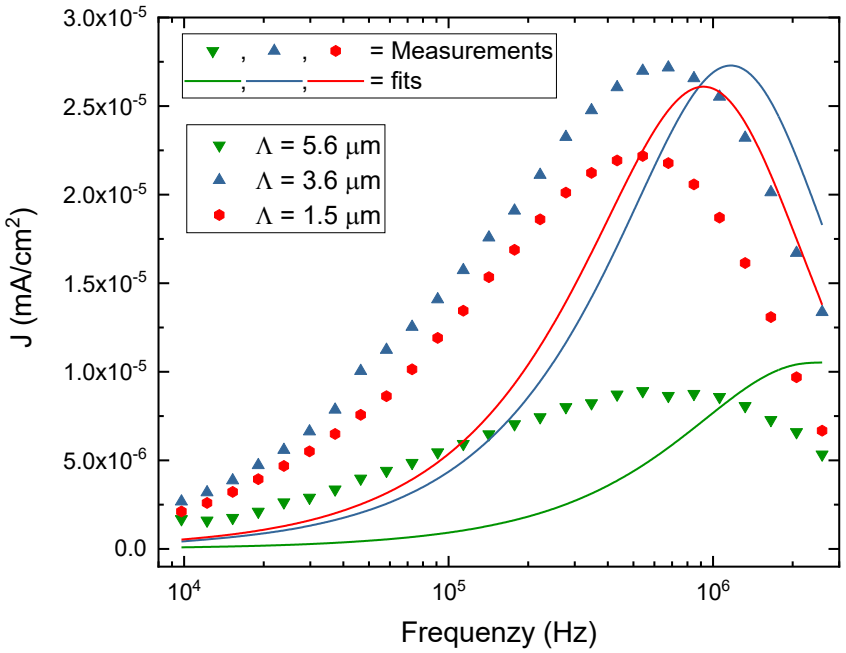


*Figure 2: Best fit obtained for a single acceptor trap level. The density of acceptor trap states is 7.2x10$^{15}$ cm$^{-3}$ located at 0.62 eV above the valence band edge, while the capture coefficients are $c_n$=7.5x10$^{-10}$ cm$^3$s$^{-1}$ and $c_p$=7.5x10$^{-9}$ cm$^3$s$^{-1}$.*

From the computer code, we obtained values that are one orders of magnitude higher. If we try to match both $\sigma_{dark}$ (controlled by the energetic position of the trap) and $\sigma_{ph}$ (mainly controlled by the capture coefficients), the MGT curves move towards even higher frequencies (shown in the supplementary information). This can be explained since the maxima of MGT curves can be related to a specific lifetime of the sample, as mentioned in previous papers [2,11]. If the conditions used in the simulation are close to the lifetime regime, the frequency at which the maxima of the curves occur give information on the lifetime of majority carriers [12]. In order to decrease the photoconductivity, we have to increase the capture coefficients, meaning that the lifetime of majority carriers diminishes, which in turn increases the frequency at which the maxima occur.

Therefore, we can conclude that this DOS model is able to reproduce only partially the measurements on this type of sample (methylammonium lead iodide sample, for further details see [2]). We may consider that the main problem comes from not being able to reproduce the maxima of the curves at the desired frequency, which is an important characteristic of MGT curves. A second issue would be that the model cannot match exactly the values of dark and photoconductivity that were measured.

Finally, it is interesting to see what happens when trying to fit the simulated MGT curves with the fitting procedure proposed by Haken *et al*. [11]. The results of this fits are shown in figure 3.

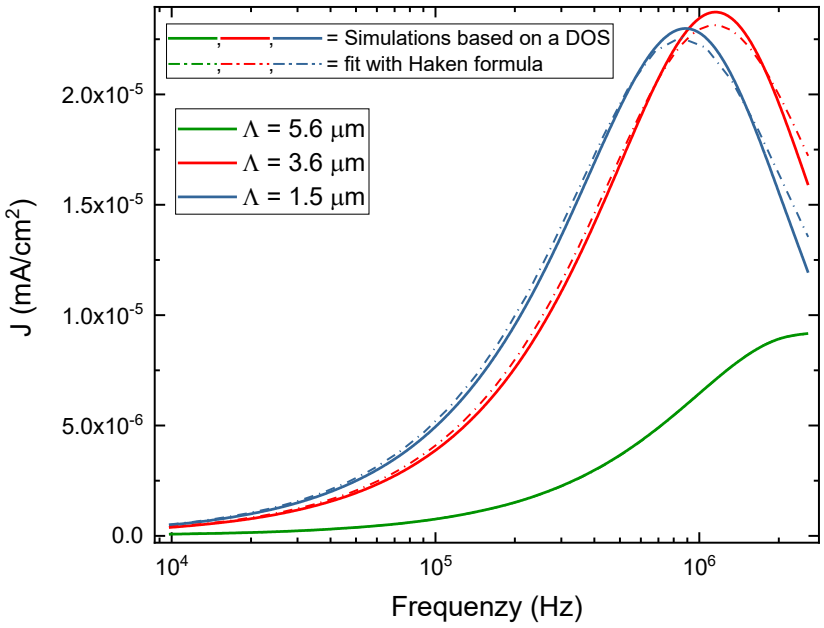


*Figure 3: MGT simulated curves using a single trap model (dotted curves) and the corresponding fit using the original method (solid lines) for the three measured grating periods.*

As it can be seen, all the curves seem to be well fitted with Eq. (1) (as was the case of figure 1a, since here we are also fitting each curve individually), the original formula proposed by Haken *et al*. What it is interesting to consider is that, having a defined density of states, we can calculate the fit parameters $\tau_R$, $\mu_N$ and $\mu_P$ from their definitions. Indeed, the solution of Eqs. (3)-(9) under a continuous (dc) illumination gives the concentration of carriers in the bands and in gap states, which in turn can be used to calculate the transport parameters.

To calculate the drift mobilities we use $\mu_N = \mu_N^0 \dfrac{n_{dc}}{n_{dc} + n_{trap}}$ [13], where $\mu_N^0$ is the extended states mobility (assumed as 0.4 $cm^2V^{-1}s^{-1}$), $n_{dc}$ is the population of electrons in the conduction band under steady state illumination, and $n_{trap}$ is the density of trapped negative charge. A similar definition can be used to calculate the holes drift mobility, while the mutual recombination lifetime $\tau_R$ can be calculated as $\tau_R = \dfrac{\sigma_{ph}}{q(\mu_N + \mu_P)G_0}$. From these definitions, the recombination lifetime resulting from the DOS chosen is $\tau_R = 0.29$ µs, while the drift mobilities are $\mu_N = 0.26$ $cm^2V^{-1}s^{-1}$ and $\mu_P = 1$ $cm^2V^{-1}s^{-1}$. This means that the holes drift mobility equals the extended states one, which can be understood taking into account that the acceptor trap can only be negatively charged (when occupied) or neutral (when empty), meaning that $p_{trap} = 0$. Regarding the values obtained from the fits with Eq. (1), we can see that $\mu_P$ takes values of 0.13, 0.22 and 0.30 $cm^2V^{-1}s^{-1}$ for increasing grating periods, while $\mu_N$ results in 0.005, 0.02 and 0.17 $cm^2V^{-1}s^{-1}$, respectively. Regarding the recombination lifetimes resulting from the fit, these are 2.0, 1.15 and 0.58 µs. Therefore, even when the three curves have been simulated with the same values of mobilities and lifetime, the fit with Eq. (1) gives parameters that depend on the grating period. The largest grating period (5.6 µm) gives the parameters closest to those calculated from the DOS: 0.30 instead of 1 $cm^2V^{-1}s^{-1}$ for $\mu_P$,

0.17 instead of 0.26 $cm^2V^{-1}s^{-1}$ for $\mu_N$, and 0.58 instead of 0.29 μs for $\tau_R$. It is thus clear that, at least for the DOS model considered here, the original model proposed by Haken *et al*. [3,11] will not give accurate results for the transport parameters, although it can still be used for comparison purposes.

**B. Gaussian defects (a-Si like)**:

The use of numerical codes, such as AMPS-1D and SCAPS, to simulate solar cells employing perovskite materials as the absorber layer, has become common in recent years. Worth mentioning are the works of Liu *et al*. [14] using AMPS-1D to optimize the thickness of the absorber layer, Minemoto and Murata [15] showing the impact of the work function of the back contact, Du *et al*. [16] studying the influence of various parameters on the solar cell performance, and Huang *et al*. [17] focusing on the improvement of electron-transport-layer free devices, to name a few. It is important to note that both simulation codes rely on the definition of the density of states for all the layers involved, so it is interesting to investigate if the DOS defined for the absorber material gives MGT curves that resemble our measured ones. We consider this point of crucial importance, since those DOS models are still being used in recent works [18–20].

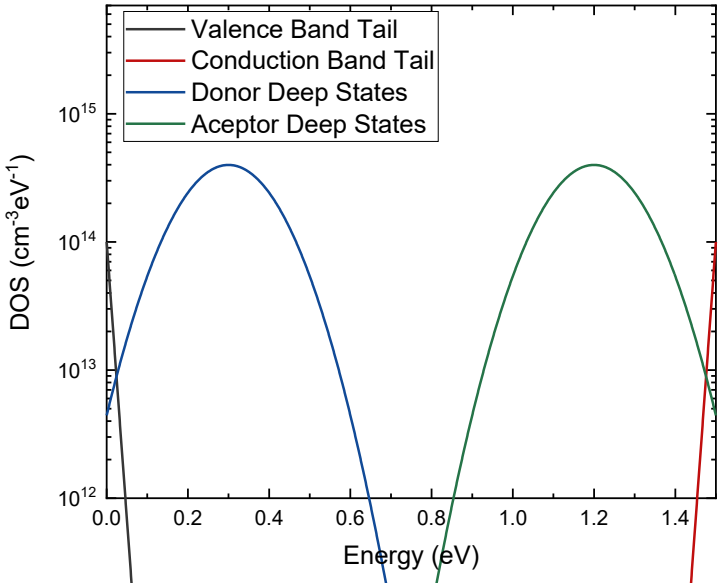


*Figure 4: Density of states chosen by Liu et al. to perform their studies. The band tails have a characteristic slope of 0.01 eV and a density of states at the band edges of $1x10^{14}$ $cm^{-3}eV^{-1}$, while the Gaussian distributions of defects are at 1.2 eV from their respective band edges, with a standard deviation of 0.1 eV and an integrated density of defects of $1x10^{14}$ $cm^{-3}$. Taken from the supplementary information of [11].*

Beginning with the work of Liu *et al*. [13, supplementary information], the chosen DOS for their work is shown in figure 4.

As it can be seen, this density of states can be considered symmetric with respect to the middle of the gap. In order to generate the characteristic p-type nature of MAPI perovskites, which later on was explained from first-principle calculations [21], the authors included a fixed concentration of ionized acceptors, $N_a$=$2.14\times10^{17}$ $cm^{-3}$. This type of density of state is reminiscent of amorphous semiconductors, being hydrogenated amorphous silicon (a-Si:H) the most widely studied. In the case of a-Si:H, the origin of the band tails was related with the spread of bonding angles between Si atoms, while the Gaussian

distributions of defects were associated with coordination defects that result in dangling bonds. In the case of perovskite materials, band tails and deep defects have also been measured [22].

Running our simulation with the parameters of Liu *et al*. [14], gives MGT current densities up to 5 orders of magnitude lower than the measured values ($2x10^{-10}$ mA/cm$^2$ compared to $\sim 1x10^{-5}$ mA/cm$^2$ for several samples measured). Moreover, both $\sigma_{dark}$ and $\sigma_{photo}$ are orders of magnitude higher compared to our case. Increasing the acceptor and donor defect concentrations to $3x10^{18}$ cm$^{-3}$, while maintaining the symmetry of the DOS, we see that the dark conductivity and photoconductivity become of the order of our measured values. However, as long as the DOS remains symmetric the MGT curves still remain around zero, so it is interesting to analyze why this happens.

In order to calculate the induced short circuit current, we should see what happens for both the internal electric field $\xi_{int}(x,t)$ and the terms $\Delta n(x,t)$ and $\Delta p(x,t)$ that come from the modulated illumination, as shown in equation (10). It can be seen that, in the case of a symmetrical distributions of states in the forbidden gap and equal band mobilities for electrons and holes, the term $\Delta\xi_{int}$ (internal electric field due to Poisson´s equation) vanishes. This happens because the terms in Eq. (5) cancel in pairs ($\Delta p(x,t) \approx \Delta n(x,t)$ and the charge trapped in acceptor states cancels with the charge trapped in donor states), leading to no field (details in the supplementary information). This effect of the MGT signal can also be seen in the original development of Ref. [11]: samples with symmetrical distributions will lead to equal drift mobilities, hence making $c_1 = 0$ in Eq. (1).

From this analysis we conclude that samples with MGT curves different from zero cannot be modelled by a symmetrical density of states with equal band mobilities. In this sense, this shows an exciting characteristic of MGT that is not shared by similar photoconductivity-based techniques such as SSPG, MPC or SSPC, for instance. Together with the ability of showing directly the semiconductor type (*n* or *p* type), a nonzero MGT curve is a clear signature that the DOS of the sample is not symmetrical.

It is also interesting to note that many works in the literature, such as those of Minemoto and Murata [15], Du *et al*. [16] and Huang *et al*. [17], use a symmetrical density of states and equal band mobilities, which according to our measurements will not describe correctly the MAPI films.

If we try to reproduce the experimental data with a DOS having two exponential band tails and two Gaussian defect states, allowing for asymmetries to achieve an internal field, the number of parameters growths rapidly. Indeed, in this case we have three parameters for each Gaussian and two parameters for each band tail, totalizing ten parameters without taking into account the capture coefficients. Proceeding in this manner, without any physical constraint, loses meaning since it is only a mathematical procedure. If we try to find good matches allowing some parameters to vary, rapidly we can find good fits, as shown in figure 5, but the lack of physical interpretation of the chosen DOS limits the analysis at this moment. It will be interesting to see if more research in this subject can provide an interpretation of deep states in the gap with Gaussian distributions.

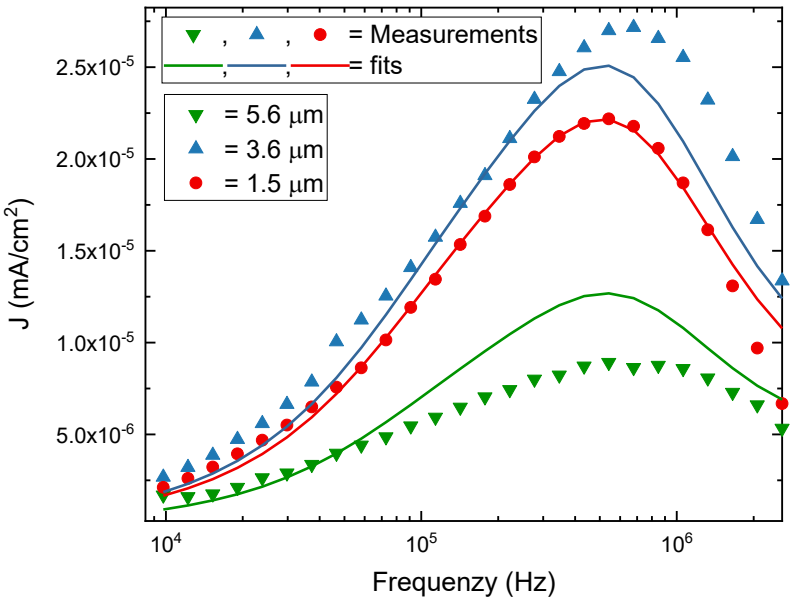


*Figure 5: Best fit obtained using a DOS model containing two wide gaussian distributions and wide band tails. The mount of parameters is so large that good fitting can be found, but extracting physical meaning of the DOS found may be challenging (full set of parameters in the SI)*

**C. Our best proposal**:

By studying the different models discussed in the previous sections, it is clear that a combination of both would be a good alternative. On the one hand, the model proposed by Levine *et al*., having a well-defined physical interpretation, is very limited in the number of parameters that can be explored to reproduce the measured MGT curves. On the other hand, the second model analyzed has the opposite problem, the number of parameters without any physical support was too large to be considered, turning the problem into a mathematical procedure that may not have a valid physical counterpart.

Recently, a possible origin for bandtail states in organic semiconductors was suggested [23]. In his work, Novikov argues that the origin of tail states in the bandgap may be due to electrostatic disorder originating from randomly located and oriented permanent dipoles and quadrupoles.

With this in mind, we propose a model with a single acceptor trap, located a few *kT* above the Fermi level (Levine´s model), with band tails defined as $Vbt(E) = N_{vt}\, e^{(-E/E_{vt})}$ for the valence band tail (considered as made of donor states) and $Cbt(E) = N_{ct}\, e^{(-(E_c-E)/E_{ct})}$ for the conduction band tail (acceptor states). Here, $N_{vt}$ and $N_{ct}$ are the densities of band tail states at the band edges, and $E_{vt}$, $E_{ct}$ are the characteristic energies. We start by proposing band tails that merge continuously with the valence and conduction bands. Regarding the characteristic energies, we start with values smaller than those accepted for hydrogenated amorphous silicon (values of ~ 0.05 eV for the conduction band tail and ~ 0.03 eV for the valence band tail [24]), and for the sake of simplicity we will use equal values for both tails. Therefore, the densities of donor and acceptor states that appear in Eq. (5) of the model are given by

$$N^{DON}(E) = N_{vt}\, e^{-\frac{E}{E_{vt}}},$$

$$N^{ACC}(E) = N_{ct}\, e^{-\frac{(E_C - E)}{E_{ct}}} + \frac{N_t}{\Delta\sqrt{2\pi}}\, e^{-\frac{(E-E_t)^2}{2\,\Delta^2}},$$

where the width of the Gaussian function has been taken as $\Delta = 0{,}01$ meV. In turn, the total density of states that appears in Eqs. (6-7) is given by

$$N(E) = N^{DON}(E) + N^{ACC}(E).$$

In figure 6 we show the fit obtained when varying 6 parameters from this model: both slopes defining the band tails ($E_{ct}$ and $E_{vt}$), the energy and density of acceptor defects ($E_t$ and $N_t$) and it capture coefficients. Regarding the density of tail states, they were set at $N_{vt} = N_{ct} = 9.35\text{x}10^{19}$ cm$^{-3}$eV$^{-1}$, which coincides with the band edges (assuming $N_{vt} = \frac{N_V}{kT}$ and $N_{ct} = \frac{N_C}{kT}$, with the values of $N_V$ and $N_C$ taken from [10]).

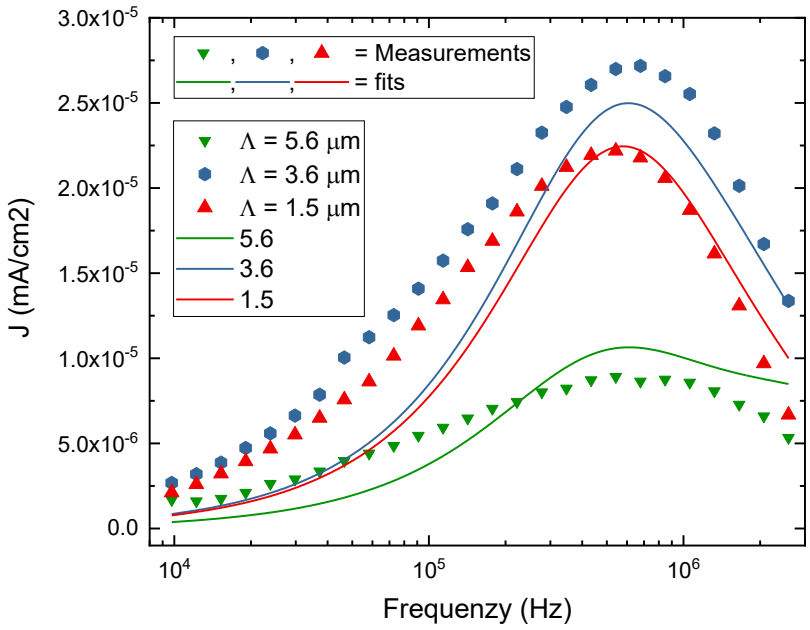


*Figure 6: Best fit obtained for a single acceptor trap level and band tail states. The density of acceptor trap states is 5x10$^{15}$ cm$^{-3}$ located at 0.6 eV above the valence band edge, while the capture coefficients are $c_n$=5x10$^{-10}$ cm$^3$s$^{-1}$ and cp=2x10$^{-9}$ cm$^3$s$^{-1}$. The band tails are both described by a characteristic energy of 0.006eV and a density of state at the band edges of 2.5x10$^{18}$ cm$^{-3}$eV$^{-1}$.*

As it can be seen, by adding the exponential band tails we get a much better fit, compared to the one shown in figure 2. The frequencies at which the maxima of the curves occur, coincide perfectly well with the measured ones, while their intensities are very close to the ones measured in the range from $10^5$ to 2x10$^6$ Hz. However, the fit is not perfect, as for lower frequencies the experimental data are always higher than the simulated ones. As explained, we fitted both slopes, reaching a value of 7.4x10$^{-3}$ meV for the valence band tail, and 2,7x10$^{-3}$ meV for the conduction one. In this case, we found a density of acceptor trap states of 4.53x10$^{15}$ cm$^{-3}$ located at 0.6 eV above the valence band edge, while the capture coefficients

are $c_n$=4.97x10$^{-10}$ cm$^3$s$^{-1}$ and $c_p$=2x10$^{-9}$ cm$^3$s$^{-1}$. As explained before, the energy location of the trap affects the Fermi level, and therefore the dark conductivity, but has little influence on the shape of the MGT curves. The value of 0.6 eV yields a Fermi level situated at 0.35 eV above the valence band edge, and $\sigma_{dark}$=1.3x10$^{-7}$ (Ωcm)$^{-1}$, which is 1 order of magnitude higher than the experimental result. In order to decrease this value, the trap should be located at 0.72 eV, which leads to a Fermi level at 0.4 eV and the correct value for $\sigma_{dark}$. Regarding $\sigma_{ph}$, it continues to be rather high, almost 1 order of magnitude higher than the experimental value. Adding the band tails does not fix this problem, since increasing the values of the capture coefficients shifts the MGT curves towards higher frequencies.

Regarding the values obtained from the fit, which are represented in the final DOS shown in figure 7, we could set boundaries to the characteristic energies, meaning that, even if the best fit was achieved with the values listed, if we constrain the fit to higher values for both slopes, the range (1x10$^{-3}$ – 1x10$^{-2}$) eV for both characteristic energies still give good fits. However, for higher values, the curve simulated for a grating period of 5.6 μm (green curve in figure 6) starts to have higher values than the other two, while for lower values we have an intensity shift between 3.6 μm (blue curve) and 1.5 μm (red curve) (the red curve goes over the blue curve). Regarding the values of the $N_{vt}$ and $N_{ct}$, we have seen that in the works cited in section 3.2 the authors use very low values for both, in the order of 10$^{14}$ cm$^{-3}$eV$^{-1}$. If we try to use lower values, we find that for $N_{vt}$ = $N_{ct}$ = 2.5x10$^{16}$ cm$^{-3}$eV$^{-1}$ the red curve (1.5 microns) goes over the blue curve (3.6 microns), and for lower values the results are even worst. This result can be taken as evidence towards higher values of $N_{vt}$ and $N_{ct}$ (closer to the DOS of the bands at the band edges).

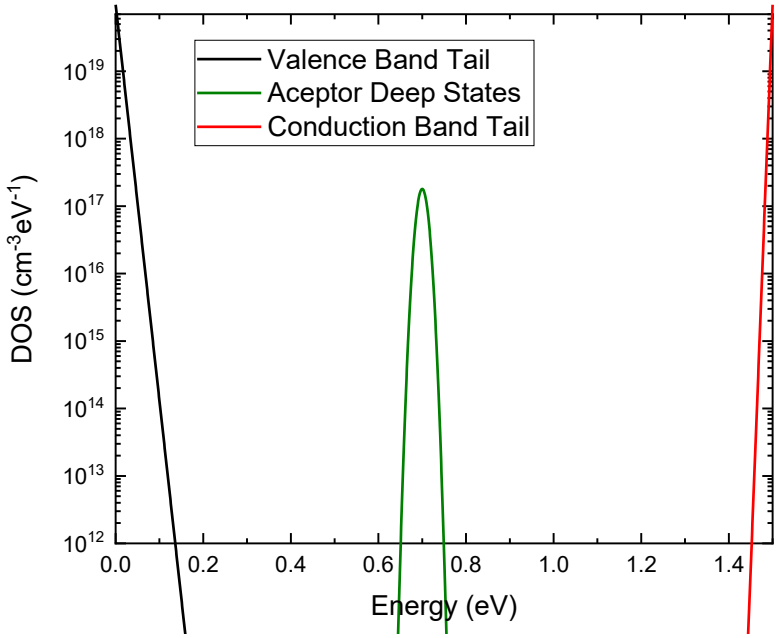


*Figure 7: Final density of states obtained with our model after fitting 6 parameters, both slopes of the exponential band tails, the energy and density of the acceptor trap and it capture coefficients.*

Finally, regarding the difference between the measured photoconductivities and those obtained from the fit, we attribute this issue to the interface between the perovskite film and the gold contacts, since it is known that gold can penetrate the perovskite film and degrade it [25]. Since the contacts and interface states are not taken into account in the designed numerical code, we estimate that part of the

photogenerated carriers are lost in recombination processes at the interfaces with the gold contacts, which is not taken into account in the simulations. This will be investigated in future experiments, for instance trying different passivating layers between the metal and the MAPI film.

## V. CONCLUSION

In the present work, we have continued exploring how the moving grating technique, a proposal done in the 90s for estimating both drift mobilities and the mutual recombination time of amorphous semiconductors, can be successfully applied to perovskite films. We have shown that the original methodology for obtaining these parameters may lead to incorrect results. In particular, we have shown that the original formula used to fit MGT curves, gives different parameters when the grating period is varied, even when they are not expected to change as long as the temperature and generation rate are kept constant. We attribute this problem to the fact that the original methodology relies on the simplification of not distinguishing between free and trapped carriers. In order to correct this issue, we have presented a more general formalism that distinguishes free and trapped carriers via the definition of a density of states in the forbidden gap. This treatment allowed us to test different models available in the literature, by means of numerical simulations. An important discovery has been that a density of states symmetrical with respect to midgap, and having equal band mobilities for electrons and holes, cannot reproduce our measurements since it gives a vanishing MGT current density. Finally, we have shown that a DOS composed of a single acceptor level located above the Fermi level, and exponential band tails that start at the band edges, gives curves that resemble the measured ones. According to our simulations, the slope of the tail states should be in the range of 0.001 - 0.01 eV, while the density of band tail states should be higher than $10^{18}$ $cm^{-3}eV^{-1}$ at the band edges. To our knowledge these are the first measurements based on steady-state techniques that give ranges for these parameters on MAPI films.

**Acknowledgement:**

The research leading to these results has received funding from the European Research Council (ERC) under the European Union's Horizon 2020 research and innovation programme (Grant agreement No. 834431) the Spanish Ministry of Science, Innovation and Universities (MINECO), PCI2019-111829-2 and CEX2019-000919-M and the Comunitat Valenciana PROMETEU/2020/077.

We also acknowledge support from the Argentinean National Scientific and Technical Research Council (CONICET) under Project PUE 22920160100054CO, and the Argentinian National Agency for Science and Technology Promotion (ANPCyT) under Projects PICT-2016-1389 and PICT-2018-1614.

## References:

[1] I. Levine, S. Gupta, A. Bera, D. Ceratti, G. Hodes, D. Cahen, D. Guo, T.J. Savenije, J. Ávila, H.J. Bolink, O. Millo, D. Azulay, and I. Balberg, Journal of Applied Physics **124**, (2018).

[2] F. Ventosinos, A. Koffman-Frischknecht, W. Herrera, M. Senno, J. Caram, M.D. Perez, and J.A. Schmidt, Journal of Physics D: Applied Physics **53**, (2020).

[3] U. Haken, M. Hundhausen, and L. Ley, Applied Physics Letters **63**, 3066 (1993).

[4] U. Haken, M. Hundhausen, and L. Ley, Physical Review B **51**, (1995).

[5] F. Ventosinos, N. Budini, C. Longeaud, and J.A. Schmidt, Journal of Physics D: Applied Physics **44**, (2011).

[6] L. Kopprio, F. Ventosinos, and J. Schmidt, Review of Scientific Instruments **90**, (2019).

[7] A. Babaei, K.P.S. Zanoni, L. Gil-Escrig, D. Pérez-del-Rey, P.P. Boix, M. Sessolo, and H.J. Bolink, Frontiers in Chemistry **7**, (2020).

[8] J.K. Arch, F.A. Rubinelli, J. -Y. Hou, and S.J. Fonash, Journal of Applied Physics **69**, 7057 (1991).

[9] M. Burgelman, P. Nollet, and S. Degrave, Thin Solid Films **361**, 527 (2000).

[10] I. Levine, S. Gupta, T.M. Brenner, D. Azulay, O. Millo, G. Hodes, D. Cahen, and I. Balberg, Journal of Physical Chemistry Letters **7**, 5219 (2016).

[11](n.d.).

[12] F. Ventosinos, C. Longeaud, and J.A. Schmidt, Journal of Non-Crystalline Solids **358**, 2031 (2012).

[13] R.H. Bube, *Photoconductivity of Solids* (J. Wiley and Sons, New York and London, 1960).

[14] F. Liu, J. Zhu, J. Wei, Y. Li, M. Lv, S. Yang, B. Zhang, J. Yao, and S. Dai, Applied Physics Letters **104**, (2014).

[15] T. Minemoto and M. Murata, Current Applied Physics **14**, 1428 (2014).

[16] H.-J. Du, W.-C. Wang, and J.-Z. Zhu, Chinese Physics B **25**, 108802 (2016).

[17] D. Li, L. Song, Y. Chen, and W. Huang, Advanced Science **7**, (2020).

[18] I. Montoya De Los Santos, H.J. Cortina-Marrero, M.A. Ruíz-Sánchez, L. Hechavarría-Difur, F.J. Sánchez-Rodríguez, M. Courel, and H. Hu, Solar Energy **199**, 198 (2020).

[19] M. Dadashbeik, D. Fathi, and M. Eskandari, Solar Energy **207**, 917 (2020).

[20] G. Haidari, AIP Advances **9**, (2019).

[21] Y. Yan, W.-J. Yin, T. Shi, W. Meng, and C. Feng, in *Organic-Inorganic Halide Perovskite Photovoltaics* (Springer International Publishing, Cham, 2016).

[22] C.M. Sutter-Fella, D.W. Miller, Q.P. Ngo, E.T. Roe, F.M. Toma, I.D. Sharp, M.C. Lonergan, and A. Javey, ACS Energy Letters **2**, (2017).

[23] S. v. Novikov, Journal of Chemical Physics **154**, (2021).

[24] R.E.I. Schropp and M. Zeman, *Amorphous and Microcrystalline Silicon Solar Cells: Modeling, Materials and Device Technology* (1998).

[25] K. Domanski, J.P. Correa-Baena, N. Mine, M.K. Nazeeruddin, A. Abate, M. Saliba, W. Tress, A. Hagfeldt, and M. Grätzel, ACS Nano **10**, (2016).